And Yet it Moves! Microfluidics Without Channels and Troughs

Francesca Lugli, Giulia Fioravanti, Denise Pattini, Luca Pasquali, Monica Montecchi, Denis Gentili, Mauro Murgia, Zahra Hemmatian, Massimiliano Cavallini, and Francesco Zerbetto**

A simple, versatile, rapid, and inexpensive procedure based on the immersion method is developed to fabricate chemical gradients on chemically activated Si/SiO_2 surfaces by a trichloro (1H,1H,2H,2H-perfluorooctyl) silane self-assembly monolayer (SAM). Contact angle measurements, atomic force microscopy, and X-ray photoelectron spectroscopy data based on the intensity of the signals of C1s and F1s, which progressively increase, indicate that the surface is characterized by the presence of increasing amounts of the SAM along the gradient direction. Experimental conditions are optimized by maximizing the variation of the contact angle of water drops at the starting and the ending points of the gradient. The application of the chemical gradient to droplet motion is demonstrated. The results are rationalized by dissipative particle dynamics simulations that well match the observed contact angles and the velocities of the drops. The simulations also show that the intrinsic nature of the gradient affects the velocity of the motion.

1. Introduction

DNA microarrays, digital lab-on-a-chip, anti-fogging devices[1] and fog-harvesting,[2] inkjet printing,[3] thin-film lubrication,[4] liquid nanodroplets spreading[5] and other technological applications in dewetting[6] share the dynamics of drops as the central component of their inner working. The dynamics of macroscopic quantities of liquids is dictated by gravity. At smaller scales, surface forces dominate.

The Marangoni flow exhibited by wine drops is perhaps one of the most celebrated examples of drop movement caused by surface forces. The surface tension of alcohol is responsible for the motion. When alcohol and water are mixed inhomogeneously, the region with a lower concentration of alcohol has a greater surface tension and pulls the fluid more strongly. The result is that the fluid tends to flow away from regions with higher alcohol concentration.

More often, the surface forces make droplets stick to their substrates even when they are inclined, which is a practical issue for windshields, windowpanes, greenhouses, and microfluidic devices. Texture can modify the wettability of surfaces and generate unusual dynamics of drops. Advancements in surface engineering, with the fabrication of various micro/nanoscale topographic features,[7] and selective chemical patterning on surfaces,[8] have enhanced surface wettability and enabled control of the liquid film thickness[9] and final wetted shape.[10] Groove geometries and the chemistry of patterned surface have produced anisotropic wetting, where contact-angle variations in different directions elongates the droplet shapes.[11] The variation of morphology of drops is usually represented in terms of contact angles and has been studied deeply.[7a,11h]

In general, liquid droplets may move in the presence of chemical gradients that can be fabricated on a solid substrate by several methods. They include chemical vapor deposition,[12] solution-controlled deposition,[13] contact printing,[14] photoirradiation,[15] photodegration,[16] and thermal-treated,[17] to name a few approaches. The gradient creates a difference in the surface tension. Movement on designed surfaces is advantageous because it does not depend on any kind of fuel. The disadvantage is that the surface must be accurately designed and fabricated.

Dr. F. Lugli, Dr. D. Pattini
Dipartimento di "Chimica G. Ciamician"
Università di Bologna
V. F. Selmi 2, 40126 Bologna, Italy
Dr. G. Fioravanti
Department of Physical and Chemical Sciences
University of L'Aquila
Via Vetoio 1, 67100 L'Aquila, Italy
Dr. L. Pasquali, Dr. M. Montecchi
IOM-CNR-, S.S. 14, Km. 163.5, Basovizza, 34149 Trieste Italy and
Dipartimento di Ingegneria
Università di Modena e Reggio Emilia
Via Vignolese 905, 41125 Modena, Italy
Dr. D. Gentili, Dr. M. Murgia, Z. Hemmatian
Istituto per lo Studio dei Materiali Nanostrutturati (ISMN)
Consiglio Nazionale delle Ricerche (CNR)
Via P. Gobetti 101 40129 Bologna, Italy
Dr. M. Cavallini
Istituto per lo Studio dei Materiali Nanostrutturati (ISMN)
Consiglio Nazionale delle Ricerche (CNR)
Via P. Gobetti 101 40129 Bologna, Italy
E-mail: m.cavallini@bo.ismn.cnr.it
Prof. F. Zerbetto
Dipartimento di "Chimica G. Ciamician"
Università di Bologna
V. F. Selmi 2, 40126 Bologna, Italy
E-mail: francesco.zerbetto@unibo.it

DOI: 10.1002/adfm.201300913

Quantitative approaches to induce drop displacement were introduced at the beginning of the 1990s,[18] and continuously refined until very recently.[19] A liquid ridge straddling a chemical discontinuity, which separated two different surfaces, gave different regimes of motion.[18a] A surface of polished silicon wafer exposed to the diffusing front of a vapor of decyltrichlorosilane had a spatial gradient in its surface free energy that caused drops of water placed on it to move uphill.[18b] The motion resulted from the imbalance of the surface tension forces acting on the liquid-solid contact line of the two opposite sides (uphill or downhill) of the drop. When the wafer was uptilted by 15° a drop of water of 1 to 2 μL at the hydrophobic end moved toward the hydrophilic end with an average velocity of approximately 1 to 2 mm per second. In order for the drop to move, the hysteresis in contact angle on the surface had to be less-than-or-equal-to 10°.[18b]

2. Surface Functionalization

In our experiments we used an immersion method that was originally developed to prepare gradients of alkanethiols self-assembled monolayers (SAMs).[20] The gradient of wettability is obtained by withdrawing a reactive surface from a diluted solution of the molecules capable to self-assemble into SAMs. **Figure 1** presents our system.

As a molecule, we used trichloro(1H,1H,2H,2H-perfluorooctyl)silane (TPOS), a highly hydrophobic molecule (i.e., water contact angle (CA) of the corresponding SAM is 109° ± 2°). As a reactive surface, we used Si/SiO_2 (native), a mildly hydrophilic surface (i.e., water CA is 48° ± 2°). The Si/SiO_2 substrate was chemically activated by a treatment at 80 °C in H_2O:H_2O_2:NH_3 and then in H_2O:H_2O_2:HCl (see details in the Experimental Section) to give a hydrophilic surface with an advancing contact angle for water <10°. The activated substrate, which usually consist of a slab of 10 × 40 mm^2, was anchored to a vertical tweeze, connected to a linear motor, and placed in a 1.0 mM solution of TPOS.

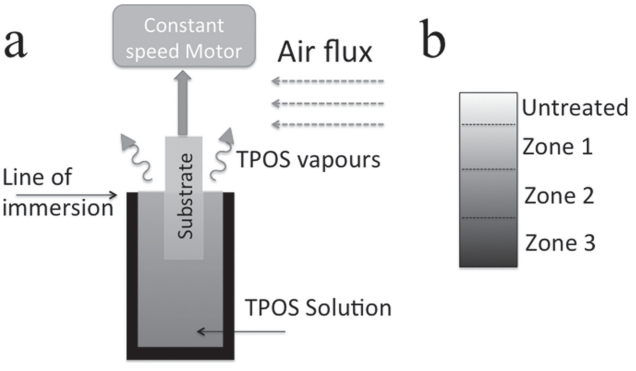

Figure 1. a) Scheme of the experimental set-up. In order to prevent the chemical reaction of the surface extracted from the solution with the vapors of TPOS we used a narrow neck vials full till the border of solvent, in this manner the TPOS vapours are immediately dispersed by the air flux of the fume hood. b) Scheme of the gradient fabricate by a. In order to show were the samples characterization were performed, samples were formally considered as three different zones with different coverage, however the real gradient is continuous along all the substrate.

In order to prevent the chemical reaction of the surface extracted from the solution with the vapors of TPOS we used a narrow neck vials full up to the border of solvent, in this manner the TPOS vapours are immediately dispersed by the air flux of the fume hood.

Immediately after immersing the surface in the TPOS solution, the motor started withdrawing the substrate out of the solution at a constant rate. The emersion of the substrates was controlled by a computer-driven linear-motion drive,[17c,21] with a constant speed of 50 μm/s. After functionalization the surface was washed with toluene, sonicated in acetone, isopropyl alcohol, and water, and dried with nitrogen.

The experiment takes no longer than 13 min and can be done in air adding the TPOS solution immediately before the beginning of the experiment. In environmental condition, with a relative humidity ranging from 40–60%, we did not observed evidence of polymerization in solution within 30 min from solution preparation; after this time the solution starts to became opalescent due to TPOS polymerization. We do not exclude the possibility of having some small aggregates of polymerized TPOS.

The samples were characterized by water contact angle (CA), atomic force microscopy (AFM) and X-ray photoelectron spectroscopy (XPS).

2.1. Surface Characterization

Samples were characterized in three different regions corresponding to the initial gradient (Zone 1, Z1, corresponding to low TPOS coverage which start from the beginning of the gradient all the way up to 1.3 cm), central gradient (Zone 2, Z2 corresponding to medium TPOS coverage, from 1.3 to 2.6 cm), and final gradient (Zone 3, Z3, corresponding to high TPOS coverage, from 2.6 to 4 cm), see Figure 1.

2.1.1. X-Ray Photoelectron Spectroscopy

Since fluorinated SAMs may degrade after prolonged exposure to X-rays, each XPS scan was acquired for a few minutes in correspondence of C1s and F1s peaks (**Figure 2**). The spectra exhibit a single broad structure centered at 689.0 eV consistent with previous data.[21] The intensity of the signals of C1s and F1s progressively increases, indicating the increasing amount of TPOS from Zone 1 to Zone 3 (Figure 2). The intensities of the different components have been calculated from the fitting procedure and are reported in **Table 1**.

2.1.2. Atomic Force Microscopy

The morphology of the wettability gradient was also investigated by AFM in intermittent contact mode. Some sub-micrometric outgrowths are occasionally present on the surface. Their origin likely depends on the partial polymerization in solution of TPOS. The number of outgrowths tends to increase with the time of immersion in TPOS solution; therefore it increases from Z1 to Z2 and Z3. It ranges between 1–2 outgrowths every 10 × 10 $μm^2$ for Z1, to 3–4 outgrowths every 10 × 10 $μm^2$ for Z2 and Z3.

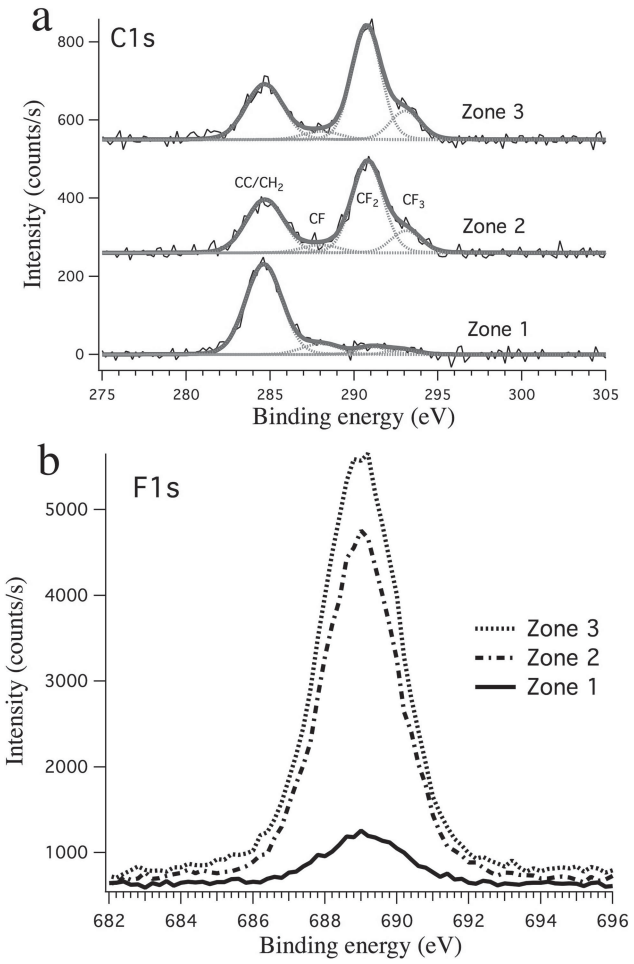

Figure 2. XPS characterization: C1s and F1s evolution in the three regions of the wettability gradient.

Table 1. XPS peak areas for the different components.

	CC/CH_2	CF	CF_2	CF_3	CF_x total	F 1s
Zone 1	646.715	79.2689	46.0371	28.7262	154.0331	1700.6
Zone 2	389.792	58.7198	562.485	132.427	753.6318	10957
Zone 3	404.242	61.1715	653.856	171.346	886.3735	13575

All regions of the samples exhibit a distribution of nanoclusters whose diameters range from 20 ± 5 nm, in Z1, to 35 ± 7 nm in the zone 3. The r.m.s. roughness changes from 1.5 nm, in Z1 to 1.1 nm in Z2 and Z3. While Z2 and Z3 appear very homogeneous (**Figure 3**a) the Z1 (low coverage) presents some larger aggregates (Figure 3b). However, zooming into these aggregates show that they are formed by a few condensed nanoclusters, which then appear as larger aggregates because of the difficulty to deconvolute entirely the effect of the AFM tip (see inset of Figure 3b).

2.1.3. Contact Angle

Experimental conditions were optimized by maximizing the variation of the CA, at the starting point of the gradient.

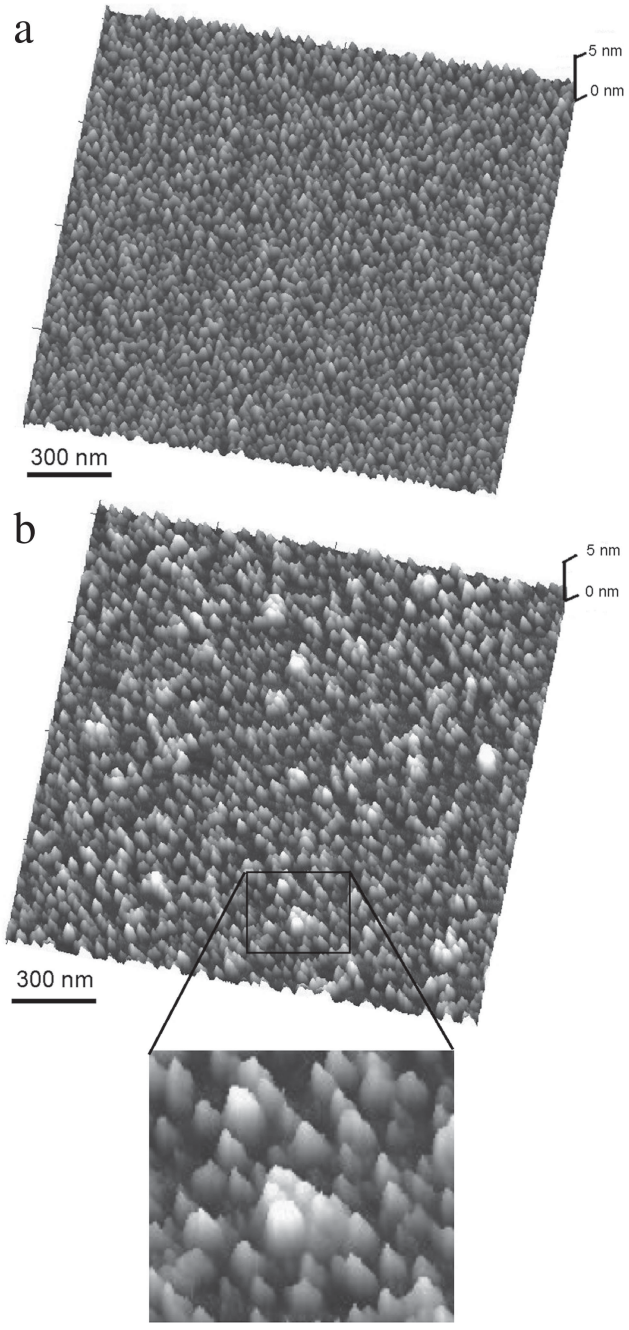

Figure 3. Typical AFM images of silicon surface functionalized by TPOS corresponding to: a) zone 3 and b) zone 1 of the samples. The inset shows a zoom of an aggregate formed by condensed nanoclusters

Figure 4 shows the effect of the chemical gradient on the static CA of water, as a function of the position along the TPOS functionalized surface. The wettability gradient varied from 107° ± 2° to 65° ± 2° (48° on bare Si/SiO_2). At high TPOS coverage, the CA almost reaches the value of complete SAM coverage (109°). The trend of CA can be fit to an exponential function, $y = a + b\exp(cx)$, where $a = 116.5° \pm 4.1°$; $b = -9.1° \pm 3.2°$; and $c = 0.4 \pm 0.1$ cm. Noticeably, although we did not perform a systematic study of the long-term aging effect, after more than

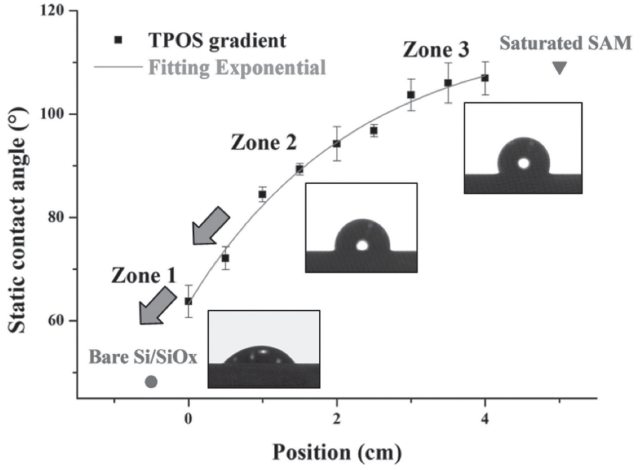

Figure 4. Static water CA measurements along the gradient and exponential fit. Measurements at 25 °C in air.

two months from preparation, the samples stored in ambient conditions, preserve their CA properties.

3. Drop Motion

Depositing a droplet of water on the functionalized surface, we observed directional movement of water droplets along the gradient without any external stimulus for CA slopes greater than 10°/mm, which was obtained in the first 10 mm of the sample (i.e., corresponding to zone 1, Figure 4). The drop displacement was 2.8 ± 0.1 mm (see **Figure 5**) in the direction of the more hydrophilic area. A movie of the droplet motion is included in the Supporting Information.

More in detail, when a drop of water (here we used 1 μL) is spread on the surface it forms a semispherical droplet, whose initial diameter depends on the position with respect to the gradient. The droplet moves spontaneously along the path gradient increasing its diameter of about 40% from the onset of the motion to its end. Because of the decrease of the CA, the height of the droplet decreases proportionally (for example in the case shown in Figure 5b the diameter changes from 1.9 mm to 2.3 mm and the height from 0.8 mm to 0.55 mm, as the CA is reduced from ≈70° to 48.3°).

Noticeably, we observed an acceleration in the first 0.5 mm reaching a maximum speed of ≈5 mm/s then, in the successive 0.5 mm it decelerates to a constant speed of ≈0.8 mm/s, which it maintains for further 0.5 mm, in the last part of the journey (13 mm) it decreases until it stops. Figure 5a shows also the trend of drop position versus time and snapshots of the droplet movement (Figure 5b).

4. Modelling

Navier-Stokes equations, also cast in the form of the lubrication model, have long been used to model drop dynamics.[22] Linearized hydrodynamic equations[23] and smoothed particle

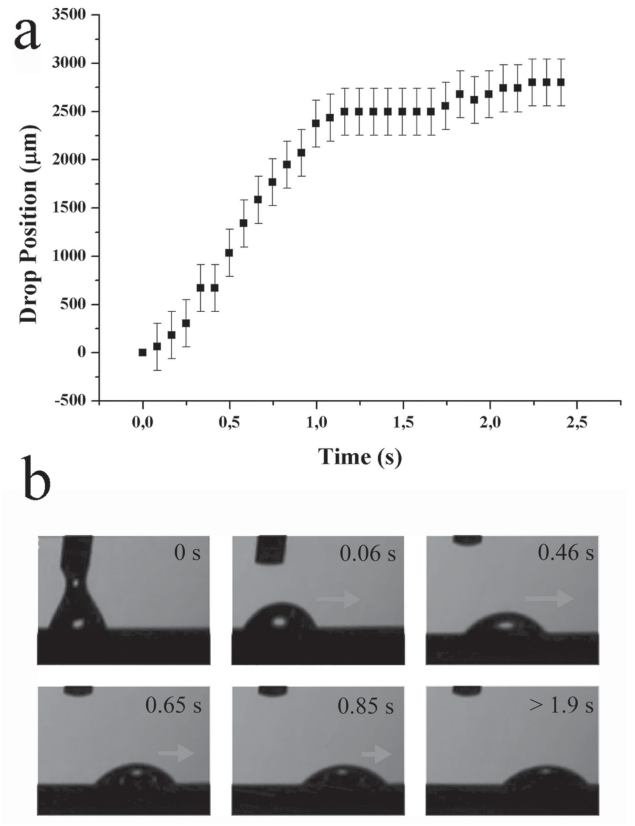

Figure 5. a) Plot of the droplet position of the drop during the movement along the gradient. b) Images of the droplet in motion. The red arrows are proportional to the velocity of the movement.

hydrodynamics were also used.[24] In terms of atomistic simulations, to the best of our knowledge, only one study has been reported.[25] Both a Lennard-Jones system and water on a SAM were investigated. For the Lennard-Jones case, the motion was steady and a simple power law described the position of its center-of-mass position with time. The behavior of the water droplet depended on the uniformity of the wetting gradient. When the gradient was nonuniform the droplet became pinned at an intermediate position. A uniform gradient with the same overall strength was able to drive a droplet of 2000 water molecules to a distance of 25 nm, which was nearly ten times its initial base radius, in tens of nanoseconds.[25]

Disspiative particle dynamics simulations[26] were carried out for a number of different drop/surface systems. The intent was to identify conditions as similar as possible to those fabricated experimentally. With a judicious choice of parameters, see **Table 2**, it was possible to reproduce semiquantitatively initial θ_i and final θ_f equilibrium contact angles and to trigger the motion of the drop from the less wettable portion to the more wettable area. To induce motion, we instantaneously modified the wettability of the surface. After equilibration of the drop, half of the area over which the drop sits was made more hydrophilic, simply by the expedient of changing the interaction parameters between the drop beads and the surface beads. All the systems considered in this study are reported in Table 2. For each case, at least three statistically

Table 2. θ_i is the initial contact angle of the drop, θ_f is the final contact angle of the drop, $\Delta\cos\theta$ accounts for the wettability gradient. Parameters *a*, *r*, *c*, and *d* correspond to the adjustable parameters of the logistic function, see caption of Figure 6.

N	θ_i	θ_f	$\Delta\cos\theta$	*a*	*r*	*c*	*d*
1	120	40	1.27	14.0	0.0860	19.3	–2.73
2	120	90	0.50	8.54	0.0645	34.0	–0.99
3	90	60	0.50	11.22	0.0717	29.1	–1.45
4	70	40	0.42	12.57	0.0587	33.9	–1.74
5	60	46	0.19	11.21	0.0389	54.7	–1.19

independent runs were carried out and the results were averaged over time and runs.

After surface modification, the drop motion is mainly unidirectional toward the direction of positive values of the *x*-axis, see **Figure 6**. The dynamics was characterized by monitoring the motion of the drop center of mass (CM). Positions and time are expressed in dimensionless DPD units; r_c is used as unit of length and $r_c = 1$. Time $t = 0$ corresponds to the instant when the surface is modified and half of the droplet surface in contact with the solid surface experiences a wettability gradient. The drop contact angle on one side changes, thus inducing a different contact angle on the other side. After reaching the hydrophilic portion of the surface, the drop motion becomes Brownian.

To further match the experiments, where aggregates are present, random chemical patterns were introduced. As depicted in **Figure 7**, the discontinuous wettability gradient was realized by randomly and increasingly modifying surface beads along the positive direction of the *x*-axis. The light grey beads of the surface in Figure 7 represents the hydrophilic aggregates evidenced by AFM experiments.

The amount of hydrophilic surface was increased as a function of *x* both linearly and exponentially. At least three independent simulations were carried out for each of the six systems considered and the results were averaged. **Figure 8**a displays the profiles of hydrophilic percentage modification along the *x*-axis of the surface. The translation motion of the droplet

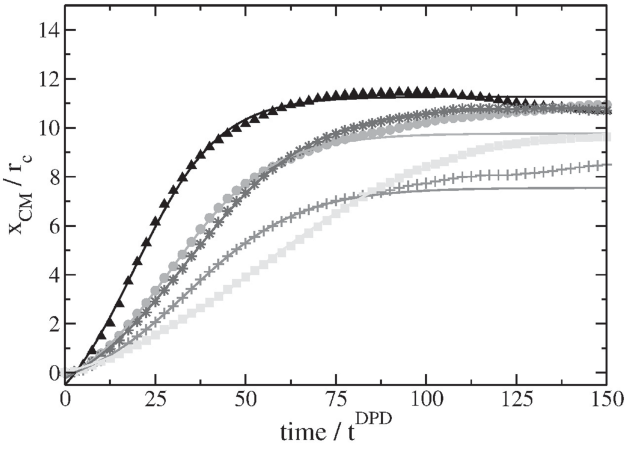

Figure 6. The results obtained from the simulations that were fitted to a logistic function, $x_{CM}(t) = \frac{a}{1+\exp\{-r(t-c)\}} + d$. The plots refers to the systems listed in Table 2: ▲ (N1), + (N2), • (N3), ★ (N4), ■ (N5).

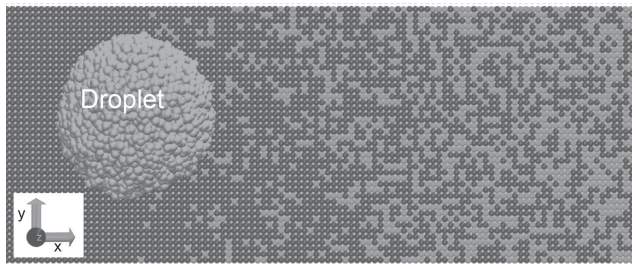

Figure 7. Random surface modification. In dark grey, hydrophobic surface portions, in light grey, hydrophilic modified surface portions. Cartesian axis are represented in the inset of the figure.

along the *x* direction is shown in Figure 8b and depends on the way the hydrophilic component builds up or in other words on the type of gradient that for simplicity is called either linear or exponential.

When the gradient is linear, the drop moves with a constant velocity towards the more hydrophilic regions. When the gradient is exponential, the drop rapidly translates to the hydrophilic region, then it slows down until it reaches equilibrium. For instance, in the system represented by the curve made of filled squares (■), the drop rapidly moves to reach a position of the center of mass *x*CM ≈ 8 rc; finally, the motion slows down

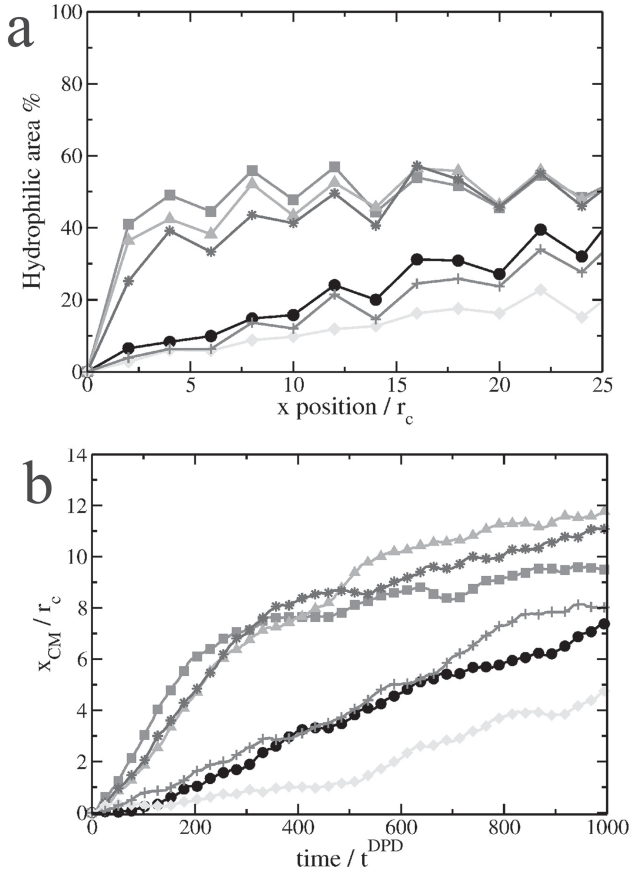

Figure 8. a) Percentage of hydrophilic component as a function of the *x* coordinate. b) Drop motion as a function of surface gradient: linear (•, +, ♦) and exponential (•, ▲, ★).

because the area of the drop in contact with the surface does not experience an effective local hydrophilic variation.

5. Conclusion

Liquid droplets move on horizontal surfaces only in the presence of a surface gradient as originally shown many years ago,[18] and continuously verified in recent years using thermal gradients[27] or a free energy ones.[28] A droplet placed on a surface gradient exhibits two differing contact angles. In the case of water, the larger contact angle is located on the more hydrophobic side of the droplet and the smaller is located on the more hydrophilic side. A difference in contact angles does not per se imply that the droplet moves. The gradient must be sufficiently small to avoid both full wetting of the surface and pinning of the drop. The wettability of the surface must therefore be prepared properly. Two of the main approaches to modify the wettability of a surface leverage on i) the introduction of chemical heterogeneities on the surface and ii) modification of surface topography by the creation of patterned or textured micro or nanoscale features.

In this work, we propose to use the immersion method using TPOS SAMs for generating simple and reproducible chemical gradient on surfaces as confirmed by CA, XPS and AFM measurements. Optimization of the procedure allows us to demonstrate droplet motion. Eventually, the results are rationalized by dissipative particle dynamics simulations that reproduce both the observed contact angles and the velocities of the drops. The simulations also show that the intrinsic nature of the gradient affects the velocity of the motion.

Here the procedure was demonstrated for a specific silane, however the proposed approach is general and can be extended to many other systems able to form SAM on different surfaces.

In order to prevent the lateral displacement of the droplets, and also drive the droplets along complex trajectories, future developments of this work will include the confinement of the gradient along lines with constant width, which could be fabricated by patterning methods (e.g., microcontact printing,[29] lithographically controlled wetting[30] or other methods[31]).

6. Experimental Section

Materials and Chemical Treatment: The wettability gradients on Si/SiO_2 were prepared from wafers of silicon with a thermally grown oxide (ca. 20 nm). The wafers were cut into pieces of ≈1.0 × 3.0 cm^2 for experiments. The pieces were rinsed heating them at 80 °C in H_2O:H_2O_2:NH_3 (5:1:1) for 5 min, rinsed with large amounts of water, them they were heated to 80 °C in H_2O:H_2O_2:HCl (6:1:1) for 5 min and rinsed again with large amounts of water. This treatment gives a hydrophilic surface with an advancing contact angle for water that is less than 10°.

The wettability gradients were then formed on these surfaces by withdrawing the surface from a freshly made 1.00 mM toluene trichloro(*1H,1H,2H,2H*-perfluorooctyl) silane (TPOS) containing solutions along the longitudinal axis of the substrate.

The emersion of the substrates was controlled by a computer-driven linear-motion drive,[17c,21] with a speed of 50 μm/s. After functionalization the surface was washed with toluene, sonicated in acetone, isopropanol and water, and dried with nitrogen.

TOPS (97%) and toluene were obtained from Aldrich and used without further purification.

Water Contact Angle Measurements: The static water contact angles of the sample surfaces were measured at 25 °C in air using a contact angle meter (GBX Digidrop instrument) on the basis of the sessile drop method. All of the contact angles were determined by averaging values measured at three different points on each sample surface. The water contact angle error was about ±2°.

The volume of the deionized (DI) water used for these measurements was 2 μL. The equivalent diameter of the spherical droplet is presumed to be 1.8 mm in the air.

Dynamic advancing and receding contact angles were measured by the motor-driven and software control instrument (Windrop).

Drop Motion Characterization: The drop motion was analysed by checking the evolution of droplets centre position from photograms extracted from the movie. The position and droplet size for each photogram was done using the open source image analysis software NIH-image. The software of GBX Digidrop instrument acquired the movie.

X-Ray Photoelectron Spectroscopy: X-ray photoelectron spectroscopy (XPS) was taken on SAMs formed on Si wafers (covered with their native oxide). Each sample consisting of a Si bar of 30 × 10 mm, with a SAM coverage gradient along the long side, was cut in three 10 × 10 pieces. These are labelled Zone 1, 2, 3 in the direction of the increasing SAM coverage.

Spectra were acquired with non-monochromatic Mg-Kα photons ($h\nu$ = 1253.6 eV) from a Vacuum Generators XR3 dual anode source operated at 15 kV, 16 mA. Photoemission data were collected with a double pass Perkin Elmer PHI 15-255G cylindrical-mirror electron analyzer. The analyzer resolution was set to 1.0 eV. The spectra are reported as a function of the electron binding energy (BE), referenced to the Au $4f_{7/2}$ signal (84 eV) of a calibration sample. A background subtraction was applied to the spectra and replicas due to Mg-Kα satellites were removed.

Morphological Characterization: AFM images were recorded with a commercial AFM (Multi-Mode 8, Bruker) operating in air (25° with relative humidity 55%). Si_3N_4 cantilevers, with typical curvature radius of a tip 10 nm were used in intermittent contact mode. Image analysis was done using the open source SPM software Gwyddion-www.gwyddion.net. In order to compensate the tilt of the image, all the presented AFM images were levelled by a second-order line.

Supporting Information

Supporting Information is available from the Wiley Online Library or from the author.

Acknowledgements

This work was supported by the project MIUR-PRIN prot. 2009N9N8RX_003.

Received: March 13, 2013
Revised: April 23, 2013
Published online: June 14, 2013

[1] a) R. Wang, K. Hashimoto, A. Fujishima, M. Chikuni, E. Kojima, A. Kitamura, M. Shimohigoshi, T. Watanabe, *Nature* **1997**, *388*, 431; b) F. C. Cebeci, Z. Z. Wu, L. Zhai, R. E. Cohen, M. F. Rubner, *Langmuir* **2006**, *22*, 2856.
[2] R. P. Garrod, L. G. Harris, W. C. E. Schofield, J. McGettrick, L. J. Ward, D. O. H. Teare, J. P. S. Badyal, *Langmuir* **2007**, *23*, 689.
[3] J. Z. Wang, Z. H. Zheng, H. W. Li, W. T. S. Huck, H. Sirringhaus, *Nat. Mater.* **2004**, *3*, 171.
[4] K. Hiratsuka, A. Bohno, H. Endo, *J. Phys. Conf. Ser.* **2007**, *89*, 012012.
[5] G. S. Grest, D. R. Heine, E. B. Webb, *Langmuir* **2006**, *22*, 4745.
[6] D. Gentili, G. Foschi, F. Valle, M. Cavallini, F. Biscarini, *Chem. Soc. Rev.* **2012**, *41*, 4430.

[7] a) D. Quere, *Rep. Prog. Phys.* **2005**, *68*, 2495; b) D. Oner, T. J. McCarthy, *Langmuir* **2000**, *16*, 7777; c) J. Bico, C. Tordeux, D. Quere, *Europhys. Lett.* **2001**, *55*, 214; d) R. Seemann, M. Brinkmann, E. J. Kramer, F. F. Lange, R. Lipowsky, *Proc. Natl. Acad. Sci. USA* **2005**, *102*, 1848; e) E. Martines, K. Seunarine, H. Morgan, N. Gadegaard, C. D. W. Wilkinson, M. O. Riehle, *Nano Lett.* **2005**, *5*, 2097.

[8] a) A. Dupuis, J. Leopoldes, D. G. Bucknall, J. M. Yeomans, *Appl. Phys. Lett.* **2005**, *87*, 024103; b) M. Gleiche, L. F. Chi, H. Fuchs, *Nature* **2000**, *403*, 173.

[9] R. Xiao, K. H. Chu, E. N. Wang, *Appl. Phys. Lett.* **2009**, *94*, 193104.

[10] L. Courbin, E. Denieul, E. Dressaire, M. Roper, A. Ajdari, H. A. Stone, *Nat. Mater.* **2007**, *6*, 661.

[11] a) F. X. Zhang, H. Y. Low, *Langmuir* **2007**, *23*, 7793; b) J. Bico, C. Marzolin, D. Quere, *Europhys. Lett.* **1999**, *47*, 220; c) Y. Chen, B. He, J. H. Lee, N. A. Patankar, *J. Colloid Interface Sci.* **2005**, *281*, 458; d) J. Y. Chung, J. P. Youngblood, C. M. Stafford, *Soft Matter* **2007**, *3*, 1163; e) H. Kusumaatmaja, R. J. Vrancken, C. W. M. Bastiaansen, J. M. Yeomans, *Langmuir* **2008**, *24*, 7299; f) J. Drelich, J. L. Wilbur, J. D. Miller, G. M. Whitesides, *Langmuir* **1996**, *12*, 1913; g) H. Gau, S. Herminghaus, P. Lenz, R. Lipowsky, *Science* **1999**, *283*, 46; h) P. G. De Gennes, F. Brochard-Wyart, D. Quere, *Capillarity and Wetting Phenomena: Drops, Bubbles, Pearls, Waves*, Springer, New York **2003**.

[12] a) Q. Liao, Y. B. Gu, X. Zhu, H. Wang, M. D. Xin, *J. Enhanced Heat Transf.* **2007**, *14*, 243; b) H. Zhao, K. Y. Law, *ACS Appl. Mater. Interfaces* **2012**, *4*, 4288; c) X. Zhu, H. Wang, Q. Liao, Y. D. Ding, Y. B. Gu, *Exp. Therm. Fluid Sci.* **2009**, *33*, 947.

[13] a) H. Elwing, S. Welin, A. Askendal, U. Nilsson, I. Lundstrom, *J. Colloid Interface Sci.* **1987**, *119*, 203; b) B. Liedberg, P. Tengvall, *Langmuir* **1995**, *11*, 3821; c) T. Uedayukoshi, T. Matsuda, *Langmuir* **1995**, *11*, 4135; d) N. V. Venkataraman, S. Zurcher, N. D. Spencer, *Langmuir* **2006**, *22*, 4184; e) M. R. Tomlinson, K. Efimenko, J. Genzer, *Macromolecules* **2006**, *39*, 9049.

[14] a) S. H. Choi, B. M. Z. Newby, *Langmuir* **2003**, *19*, 7427; b) L. Pardo, W. C. Wilson, T. J. Boland, *Langmuir* **2003**, *19*, 1462; c) A. Y. Sankhe, B. D. Booth, N. J. Wiker, S. M. Kilbey, *Langmuir* **2005**, *21*, 5332; d) T. Kraus, R. Stutz, T. E. Balmer, H. Schmid, L. Malaquin, N. D. Spencer, H. Wolf, *Langmuir* **2005**, *21*, 7796; e) M. Geissler, P. Chalsani, N. S. Cameron, T. Veres, *Small* **2006**, *2*, 760.

[15] a) S. V. Roberson, A. J. Fahey, A. Sehgal, A. Karim, *Appl. Surf. Sci.* **2002**, *200*, 150; b) R. Klauser, C. H. Chen, M. L. Huang, S. C. Wang, T. J. Chuang, M. Zharnikov, *J. Electron. Spectrosc.* **2005**, *144*, 393; c) A. Larsson, B. Liedberg, *Langmuir* **2007**, *23*, 11319; d) B. P. Harris, A. T. Metters, *Macromolecules* **2006**, *39*, 2764; e) N. Ballav, A. Shaporenko, A. Terfort, M. Zharnikov, *Adv. Mater.* **2007**, *19*, 998; f) N. Blondiaux, S. Zurcher, M. Liley, N. D. Spencer, *Langmuir* **2007**, *23*, 3489.

[16] Y. Ito, M. Heydari, A. Hashimoto, T. Konno, A. Hirasawa, S. Hori, K. Kurita, A. Nakajima, *Langmuir* **2007**, *23*, 1845.

[17] a) L. Ionov, A. Sidorenko, M. Stamm, S. Minko, B. Zdyrko, V. Klep, I. Luzinov, *Macromolecules* **2004**, *37*, 7421; b) E. Svetushkina, N. Puretskiy, L. Ionov, M. Stamm, A. Synytska, *Soft Matter* **2011**, *7*, 5691; c) S. Morgenthaler, S. W. Lee, S. Zurcher, N. D. Spencer, *Langmuir* **2003**, *19*, 10459.

[18] a) T. Ondarcuhu, M. Veyssie, *J. Phys. II* **1991**, *1*, 75; b) M. K. Chaudhury, G. M. Whitesides, *Science* **1992**, *256*, 1539.

[19] X. J. Han, L. Wang, X. J. Wang, *Adv. Funct. Mater.* **2012**, *22*, 4533.

[20] a) S. M. Morgenthaler, S. Lee, N. D. Spencer, *Langmuir* **2006**, *22*, 2706; b) M. Cavallini, M. Bracali, G. Aloisi, R. Guidelli, *Langmuir* **1999**, *15*, 3003; c) M. Cavallini, G. Aloisi, M. Bracali, R. Guidelli, *J. Electroanal. Chem.* **1998**, *444*, 75; d) M. Cavallini, R. Lazzaroni, R. Zamboni, F. Biscarini, D. Timpel, F. Zerbetto, G. J. Clarkson, D. A. Leigh, *J. Phys. Chem. B* **2001**, *105*, 10826.

[21] J. M. Gorham, A. K. Stover, D. H. Fairbrother, *J. Phys. Chem. C* **2007**, *111*, 18663.

[22] a) L. W. Schwartz, R. R. Eley, *J. Colloid Interface Sci.* **1998**, *202*, 173; b) B. U. Felderhof, *J. Chem. Phys.* **2006**, *125*, 124904; c) F. Girard, M. Antoni, S. Faure, A. Steinchen, *Langmuir* **2006**, *22*, 11085.

[23] A. Onuki, K. Kanatani, *Phys. Rev. E* **2005**, *72*, 066304.

[24] A. K. Das, P. K. Das, *Langmuir* **2009**, *25*, 11459.

[25] J. D. Halverson, C. Maldarelli, A. Couzis, J. Koplik, *J. Chem. Phys.* **2008**, *129*, 164708.

[26] a) R. D. Groot, P. B. Warren, *J. Chem. Phys.* **1997**, *107*, 4423; b) R. D. Groot, T. J. Madden, *J. Chem. Phys.* **1998**, *108*, 8713; c) P. J. Hoogerbrugge, J. M. V. A. Koelman, *Europhys. Lett.* **1992**, *19*, 155; d) P. Espanol, P. Warren, *Europhys. Lett.* **1995**, *30*, 191; e) T. Soddemann, B. Dunweg, K. Kremer, *Phys. Rev. E* **2003**, *68*, 046702; f) F. Lugli, E. Brini, F. Zerbetto, *J. Phys. Chem. C* **2012**, *116*, 592; g) M. Calvaresi, M. Dallavalle, F. Zerbetto, *Small* **2009**, *5*, 2191.

[27] a) S. J. D. D'Alessio, J. P. Pascal, H. A. Jasmine, K. A. Ogden, *J. Fluid Mech.* **2010**, *665*, 418; b) S. H. Hu, J. J. Yan, J. S. Wang, Y. Li, J. P. Liu, *Int. J. Multiphase Flow* **2007**, *33*, 935; c) H. Kitahata, N. Yoshinaga, K. H. Nagai, Y. Sumino, *Phys. Rev. E* **2011**, *84*, 015101; d) A. Onuki, *Phys. Rev. E* **2009**, *79*,046311; e) I. R. Stan, M. Tomoaia-Cotisel, A. Stan, *Rom. Rep. Phys.* **2009**, *61*, 451; f) R. Tadmor, *J. Colloid Interface Sci.* **2009**, *332*, 451; g) M. Tomoaia-Cotisel, E. Gavrila, I. Albu, I. R. Stan, *Stud. Univ. Babes-Bol. Chem.* **2007**, *52*, 7; h) X. P. Xu, T. Z. Qian, *Phys. Rev. E* **2012**, *85*, 051601; i) F. Zhang, Y. T. Wu, R. Geng, Z. B. Zhang, *Int. J. Multiphase Flow* **2008**, *34*, 13.

[28] a) O. Bliznyuk, J. R. T. Seddon, V. Veligura, E. S. Kooij, H. J. W. Zandvliet, B. Poelsema, *ACS Appl. Mater. Interfaces* **2012**, *4*, 4141; b) O. Bliznyuk, H. P. Jansen, E. S. Kooij, H. J. W. Zandvliet, B. Poelsema, *Langmuir* **2011**, *27*, 11238; c) S. Daniel, S. Sircar, J. Gliem, M. K. Chaudhury, *Langmuir* **2004**, *20*, 4085; d) A. K. Das, P. K. Das, *Langmuir* **2010**, *26*, 9547; e) G. P. Fang, W. Li, X. F. Wang, G. J. Qiao, *Langmuir* **2008**, *24*, 11651; f) J. Genzer, *Annu. Rev. Mater. Res.* **2012**, *42*, 435; g) J. Genzer, *J. Adhesion* **2005**, *81*, 417; h) Y. H. Lai, M. H. Hsu, J. T. Yang, *Lab Chip* **2010**, *10*, 3149; i) Y. H. Lai, J. T. Yang, D. B. Shieh, *Lab Chip* **2010**, *10*, 499; j) Q. Liao, H. Wang, X. Zhu, M. W. Li, *Sci. China Ser. E-Technol. Sci.* **2006**, *49*, 733; k) S. Morgenthaler, C. Zink, N. D. Spencer, *Soft Matter* **2008**, *4*, 419; l) N. Moumen, R. S. Subramanian, J. B. McLaughlin, *Langmuir* **2006**, *22*, 2682; m) S. Neuhaus, C. Padeste, N. D. Spencer, *Langmuir* **2011**, *27*, 6855; n) S. Neuhaus, N. D. Spencer, C. Padeste, *ACS Appl. Mater. Interfaces* **2012**, *4*, 123; o) S. K. Oh, M. Nakagawa, K. Ichimura, *J. Mater. Chem.* **2002**, *12*, 2262; p) R. J. Petrie, T. Bailey, C. B. Gorman, J. Genzer, *Langmuir* **2004**, *20*, 9893; q) D. M. Spori, T. Drobek, S. Zurcher, N. D. Spencer, *Langmuir* **2010**, *26*, 9465; r) T. Wu, K. Efimenko, P. Vlcek, V. Subr, J. Genzer, *Macromolecules* **2003**, *36*, 2448; s) L. Xu, Z. G. Li, S. H. Yao, *Appl. Phys. Lett.* **2012**, *101*, 064101; t) J. T. Yang, J. C. Chen, K. J. Huang, J. A. Yeh, *J. Microelectromech. Syst.* **2006**, *15*, 697–707; u) J. L. Zhang, Y. C. Han, *Langmuir* **2007**, *23*, 6136; v) B. Bhushan, Y. C. Jung, *Ultramicroscopy* **2007**, *107*, 1033.

[29] Y. N. Xia, G. M. Whitesides, *Annu. Rev. Mater. Sci.* **1998**, *28*, 153.

[30] a) M. Cavallini, D. Gentili, P. Greco, F. Valle, F. Biscarini, *Nat. Protocols* **2012**, *7*, 1668; b) M. Cavallini, I. Bergenti, S. Milita, J. C. Kengne, D. Gentili, G. Ruani, I. Salitros, V. Meded, M. Ruben, *Langmuir* **2011**, *27*, 4076; c) M. Cavallini, C. Albonetti, F. Biscarini, *Adv. Mater.* **2009**, *21*, 1043.

[31] a) M. Cavallini, *J. Mater. Chem.* **2009**, *19*, 6085; b) M. Cavallini, M. Facchini, M. Massi, F. Biscarini, *Synth. Met.* **2004**, *146*, 283; c) F. C. Simeone, C. Albonetti, M. Cavallini, *J. Phys. Chem. C* **2009**, *113*, 18987; d) M. Cavallini, J. Gomez-Segura, C. Albonetti, D. Ruiz-Molina, J. Veciana, F. Biscarini, *J. Phys. Chem. B* **2006**, *110*, 11607.